Int. J. Heat Mass Transfer. Vol. 35, No. 4, pp. 783–793, 1992
Printed in Great Britain

0017–9310/92 $5.00+0.00
Pergamon Press plc

# Simulation of unsteady-state thermocapillary mass transfer for laser doping of metals

A. A. UGLOV, I. YU. SMUROV, K. I. TAGUIROV and A. G. GUSKOV
A. A. Baikov Institute of Metallurgy, Moscow, 117911, Russia

(*Received* 7 *May* 1990)

**Abstract**—By imposing the approximation of a shallow melt bath, small reduced Reynolds number and of a plane free surface, unsteady-state thermocapillary flow of melt is considered for the case of melting a metallic solid body by a Gaussian surface heat source. Based on the velocity field obtained, convective mass transfer of the doping impurity is analysed by the method of model particles in the assumption of a small Schmidt number. The feasibility of producing both a relatively homogeneous and an essentially non-monotonous (layered) structure of concentration fields in the remelted zone is shown. The analysis of the formation of such structures is made and their specific features are revealed in the case of laser doping of metals from the gas (plasma) phase and from previously deposited coatings. Comparison between the predicted concentration profiles and the results of experiments is made and their satisfactory qualitative agreement is obtained.

## INTRODUCTION

LASER doping, which allows one to change the chemical composition of surface layers and, consequently, the properties of materials being treated, is a promising technological process [1]. It offers the opportunity for devising wear-, heat- and corrosion-resistant layers on the surfaces of metals and alloys. However, wide use of the processes of laser doping is to a certain extent restrained by the inadequate knowledge of diverse physico-chemical processes taking place in the laser-affected zone. These are: melting superseded subsequently by solidification; motion of the melt under the action of one force or another; the access and the subsequent distribution of the doping element over the lasing zone, etc. Their study entails great experimental (locality, high rates) and theoretical (simulation of the simultaneous convective heat and mass transfer problem) difficulties. The present work is aimed at mathematical simulation of the processes of heat and mass transfer in the case of laser doping over the range of moderate energy flux densities, $q \leqslant 5 \times 10^5$ W cm$^{-2}$.

Among the hydrodynamic processes occurring in the melt during laser fusion of solid bodies in the absence of extensive surface evaporation, the basic one is the thermocapillary mechanism of convection attributable to shear stresses originating on the surface of the liquid in the case of its inhomogeneous heating [2]. The use of laser radiation for initiating thermocapillary flows provides a unique possibility for studying fundamental physical laws of the given phenomenon within a wide range of parameters, since substantial temperature gradients and, consequently, high flow velocities can be realized in the lasing zone. Apart from intrinsic scientific interest, the knowledge of these laws is of great practical value for determining the optimal regimes of laser doping, laser-plasma synthesis of nitrides and carbides of refractory metals, welding, laser amorphization, and other technological processes with the formation of a liquid phase [1]. As a rule, it is necessary to determine the flow velocity field of the melt at different time instants and the depth of penetration of doping elements into the material, as well as to study the possibility of controlling these parameters by selecting the regimes of laser effect.

The surface tension of the majority of liquids (both pure elements and different solutions) depends on the interface temperature, and usually (in the absence of surfactant admixtures) it decreases with an increase in temperature [3]. This leads to the appearance of tangential stresses on the non-uniformly heated free surface of the liquid that set the liquid into motion in the direction of decreasing temperature [4]. On those rare occasions when the surface tension increases with temperature (for example, in the presence of surfactants [5]), the direction of the thermocapillary force and, consequently, the direction of the thermocapillary flow, change in the opposite manner [6]. Simple evaluations as well as experimental investigations of thermocapillary flows in liquid layers [7, 8] and in melting solid bodies [6] show that in metals exposed to laser irradiation the rates of thermocapillary convection of the melt may attain appreciable values and thus exert a substantial influence on the heat and mass transfer processes.

Despite the great attention paid in the literature to the Marangoni effect, the unsteady-state convection in melting has not as yet been sufficiently studied. When mathematical models are constructed, the attention is usually restricted for convenience to an infinite liquid layer with a fixed plane bottom [7, 9–12] or to the flows in square [13] or rectangular [14–16] cuvettes. However, these approaches have a substantial quali-

## NOMENCLATURE

$a_1, a_2$ thermal conductivities of liquid and solid phases [$cm^2 s^{-1}$]
$k$ concentration factor [$cm^{-2}$]
$L$ specific latent heat of melting [$J g^{-1}$]
$p$ pressure [dyne $cm^{-2}$]
$Pr$ Prandtl number, $v/a_1$
$q$ absorbed heat flux density [$W cm^{-2}$]
$r$ radial cylindrical coordinate [cm]
$r_f$ radius of focusing spot, $k^{-1/2}$ [cm]
$R$ radius of melt bath [cm]
$Re^*$ reduced Reynolds number, $(v_r R/v)(S/R)^2$
$s$ coordinate of melting front in one-dimensional statement [cm]
$S$ position of melting front in spatial statement [cm]
$t$ time [s]
$t_m$ instant of melting onset [s]
$T_1, T_2$ temperatures of liquid and solid phases [K]
$T_m$ melting temperature [K]
$T_0$ initial temperature [K]
$u_1, u_2$ temperatures of liquid and solid phases in one-dimensional statement [K]
$v_r, v_z$ radial and axial flow velocities [$cm s^{-1}$]
$z$ axial cylindrical coordinate [cm].

Greek symbols
$\alpha$ $-d\sigma/dT$ [dyne $cm^{-1} K^{-1}$]
$\eta$ coefficient of dynamic viscosity [$g cm^{-1} s^{-1}$]
$\lambda_1, \lambda_2$ thermal conductivities of liquid and solid phases, respectively [$W cm^{-1} K^{-1}$]
$\nu$ coefficient of kinematic viscosity [$cm^2 s^{-1}$]
$\xi$ coordinate in one-dimensional problem of melting [cm]
$\rho$ density [$g cm^{-3}$]
$\sigma$ coefficient of surface tension [dyne $cm^{-1}$]
$\tau$ time in one-dimensional problem of melting [s]
$\tau_m$ instant of onset of one-dimensional melting [s].

tative drawback: in the case of unsteady-state melting, the shape and dimensions of streamlines vary with time due to the increase in the molten pool and, consequently, the trajectories of the liquid particles also vary, since both the molten pool geometry and its volume change. This means that the study of the unsteady-state thermocapillary convection in the material being melted requires further development along the lines of considering the influence of evolution of the molten pool shape and, in the first place, of its dimensions on the velocity field.

This paper considers thermocapillary convection with a small reduced Reynolds number and the mass transfer of admixture in a shallow molten pool with allowance for the unsteady-state nature of the process of melting in application to laser treatment of melts.

## CALCULATION OF UNSTEADY-STATE MELTING

Consider the problem of melting of a semi-infinite solid body by a surface heat source in spatial statement. In the cylindrical coordinate system the phase interface is described by the equation

$$z = S(r, t)$$

where $t$ is the time, $r$ and $z$ are the radial and axial cylindrical coordinates (the $z$ axis is directed into the metal), whereas the function $S(r, t)$ is being determined in the process of problem solution. It will be assumed that the melt formed is quiescent, the coefficients of thermal conductivity and thermal diffusivity of the liquid and solid phases are constant and, generally speaking, are different, whereas a constant temperature, equal to the melting temperature $T_m$, is maintained at the melting front:

$$T_1(r, z = S, t) = T_2(r, S, t) = T_m \tag{1}$$

where $T_i$ is the temperature of the liquid ($i = 1$) and of the solid ($i = 2$) phases.

The energy flux density absorbed on the surface $z = 0$ is constant and is determined according to the law:

$$-\lambda_1 \left.\frac{\partial T_1}{\partial z}\right|_{z=0} = q(r), \quad r \in \Omega \tag{2}$$

$$-\lambda_2 \left.\frac{\partial T_2}{\partial z}\right|_{z=0} = q(r), \quad r \notin \Omega \tag{3}$$

where $\Omega(t)$ is the region on the surface $z = 0$ occupied by the liquid phase; $\lambda_i$ are the thermal conductivity coefficients. The approach at hand is of use for an arbitrary (including non-monotonous) law of distribution of $q(r)$, but in what follows only the monotonically decreasing dependence of $q$ on $r$ will be considered and therefore it is assumed that $q = q_0 \times \exp(-kr^2)$. The Stefan boundary condition is given at the melting front:

$$-\lambda_1 \left.\frac{\partial T_1}{\partial n}\right|_{z=S} = -\lambda_2 \left.\frac{\partial T_2}{\partial n}\right|_{z=S} + \rho L \frac{\partial n}{\partial t} \tag{4}$$

where $\mathbf{n}(r,t)$ is the vector of the normal to the phase

interface, $\rho$ is the density and $L$ is the specific heat of melting.

Assume that the molten pool is shallow, $S \ll r_f \sim K^{-1/2}$, and consider the time instants $t \ll r_f^2/a_i$, where $a_i$ are the thermal diffusivity coefficients. Then $\partial S/\partial r \ll 1$; $\partial T_i/\partial r \ll \partial T_i/\partial z$; $\partial^2 T_i/\partial r^2 \sim (1/r)\partial T/\partial r \ll \partial^2 T_i/\partial z^2$, and the heat conduction equation and condition (4) may be written in the form

$$\frac{1}{a_1}\frac{\partial T_1}{\partial t} = \frac{\partial^2 T_1}{\partial z^2} \tag{5}$$

$$\frac{1}{a_2}\frac{\partial T_2}{\partial t} = \frac{\partial^2 T_2}{\partial z^2} \tag{6}$$

$$-\lambda_1 \frac{\partial T_1}{\partial z}\bigg|_{z=S} = -\lambda_2 \frac{\partial T_2}{\partial z}\bigg|_{z=S} + \rho L \frac{\partial S}{\partial t}. \tag{7}$$

The boundary (when $z \to \infty$) and initial conditions are

$$T_2(r, \infty, t) = T_0, \quad T_2(r, z, 0) = T_0. \tag{8}$$

The substitution of the variables $z = \xi q_0/q$, $t = \tau(q_0/q)^2$, $S(r, t) = s(\tau)q_0/q$, $T_i(r, z, t) = u_i(\xi, \tau)$ yields for the functions $u_i$ and $s$ the one-dimensional (in the variable $\xi$) problem of melting of a semi-infinite solid body by a homogeneous and time-constant surface heat source with the absorbed flux density $q_0$:

$$\frac{1}{a_1}\frac{\partial u_1}{\partial \tau} = \frac{\partial^2 u_1}{\partial \xi^2} \quad \text{when} \quad 0 < \xi < s(\tau)$$

$$\frac{1}{a_2}\frac{\partial u_2}{\partial \tau} = \frac{\partial^2 u_2}{\partial \xi^2} \quad \text{when} \quad s(\tau) < \xi < \infty$$

$$-\lambda_1 \frac{\partial u_1}{\partial \xi}\bigg|_{\xi=s} = -\lambda_2 \frac{\partial u_2}{\partial \xi}\bigg|_{\xi=s} + \rho L \frac{\mathrm{d}s}{\mathrm{d}\tau}$$

$$u_1(s, \tau) = u_2(s, \tau) = T_m$$

$$-\lambda_1 \frac{\partial u_1}{\partial \xi}\bigg|_{\xi=0} = q_0$$

$$u_2(\infty, \tau) = u_2(\xi, 0) = T_0. \tag{9}$$

The system of equations (9) involves the heating stage $\tau \leqslant \tau_m$ when $s = 0$, $\mathrm{d}s/\mathrm{d}\tau = 0$, since, as can be readily seen, problem (3), (6), (8) is reduced, with the help of the above-indicated system of variables, to the corresponding one-dimensional problem of heating of a body.

The solution of problem (9) can be obtained both analytically [17] and numerically [18].

The melting begins at the point $r = 0$. The location of the boundary of the region $\Omega$ is determined by the equation $S = 0$ or $s(\tau) = 0$, i.e. $\tau = \tau_m = (\pi/a_2) \times [\lambda_2(T_m - T_0)/2q_0]^2$. Therefore, the radius of the molten pool is $R(t) = [(1/2k)\ln(t/t_m)]^{1/2}$. At the initial stage of melting the molten pool radius increases sharply, but later the rate of its growth decreases, since the flux density $q(R)$ decreases with an increase in $R$ and, consequently, the energy spent for melting at the points $r = R$ per unit time decreases.

This means of melting calculation can be used for the cases of arbitrary (different from the Gaussian one) law of the three-dimensional energy flux density distribution within the scope of the assumptions made. In particular, the minimal characteristic dimension of the change of $q$ should substantially exceed the depth of the zone of thermal effect. Therefore, strictly speaking, this approach is inapplicable for taking into account the fine-scale structure of laser effect. However, it should be noted that appreciable differences in the heat flux densities at small distances $d$ generate high values of the temperature gradients $\partial T/\partial r$, i.e. of heat fluxes in the plane $z = 0$ that tend to smooth out the temperature over corresponding small portions of the surface for the time of order $d^2/a_i$. When $d^2/a_i \ll t$, then in such cases there is the possibility of considering the melting of a body by a heat flux averaged over fine-scale structure of a laser pulse.

## THERMOCAPILLARY FLOW VELOCITY FIELD

Consider a cylindrically symmetric thermocapillary flow in the case of melting a metallic solid body by laser radiation with the formation of a shallow molten pool $S \ll R$. In this case the times $t < t_b$ will be considered, where $t_b$ is the instant of the attainment of the boiling temperature on the surface, since with $t \geqslant t_b$ a developed evaporation from the surface occurs, resulting in large pressure gradients of metal vapours that generate forced convection which may exert a strong effect on the character of liquid motion [1].

It will be assumed that the free surface of the melt is planar, the coefficients of the dynamic ($\eta$) and kinematic ($\nu$) viscosities are constant and the coefficient of surface tension depends linearly on temperature, $\sigma(T) = \sigma_0 - \alpha T$, where usually $\alpha > 0$. Moreover, the flows will be considered with a small reduced Reynolds number, $Re^* = (v_r R/\nu)(S/R)^2 \ll 1$ ($v_r$ is the projection of the flow velocity onto the coordinate axis $r$). Then $Re^*\,Pr \ll 1$ too, since liquid metals are characterized by a small Prandtl number, $Pr = \nu/a_i \ll 1$. This means that heat conduction in a shallow pool predominates over convective heat transfer. The thermal problem governs the hydrodynamic problem, which in this approximation, in turn, does not exert the inverse effect on the thermal problem. Therefore in order to determine the shape of the molten pool $S(r, t)$ and the surface temperature $T_1(r, 0, t)$, the above-described approach can be used.

Neglecting the convective acceleration in the Navier–Stokes equations and using the thin layer approximation $v_z \ll v_r$ ($v_z$ is the projection of the flow velocity onto the coordinate axis $z$) yields the mathematical formulation of the problem:

$$\frac{\partial v_r}{\partial t} = -\frac{1}{\rho}\frac{\partial P}{\partial r} + \nu \frac{\partial^2 v_r}{\partial z^2} \tag{10}$$

$$\frac{\partial v_z}{\partial t} = -\frac{1}{\rho}\frac{\partial P}{\partial z} + \nu \frac{\partial^2 v_z}{\partial z^2} \tag{11}$$

$$\frac{1}{r}\frac{\partial}{\partial r}(rv_r)+\frac{\partial v_z}{\partial z}=0 \tag{12}$$

$$\frac{\partial v_r}{\partial z}=f(r,t),\quad z=0 \tag{13}$$

$$v_r(r,S,t)=v_z(r,S,t)=v_z(r,0,t)=0. \tag{14}$$

Here $p(r, z, t)$ is the pressure, $f(r, t)=(\alpha/\eta)\partial T_1(r, 0, t)/\partial r$. Differentiating equation (10) with respect to $z$ and equation (11) with respect to $r$ and then substracting the latter from the former (this procedure is equivalent to the application of the operation root to the vector equation of motion) and going over to the variables $\xi$ and $\tau$, problem (10)–(14) can be reduced to:

$$\frac{\partial\varphi}{\partial\tau}=\nu\frac{\partial^2\varphi}{\partial\xi^2} \tag{15}$$

$$\varphi(0,\tau)=g(\tau) \tag{16}$$

$$\int_0^s \mathrm{d}\xi\int_\xi^s \varphi(\xi_1,\tau)\,\mathrm{d}\xi_1=0, \tag{17}$$

where

$$\varphi(\xi,\tau)=(\eta/2\alpha)(\partial v_r/\partial z-\partial v_z/\partial r)q(r)/(\mathrm{d}q/\mathrm{d}r)$$
$$\simeq(\eta/2\alpha)(\partial v_r/\partial z)q(r)/(\mathrm{d}q/\mathrm{d}r),$$
$$g(\tau)=\tau\partial u_1(0,\tau)/\partial\tau.$$

To obtain an approximate solution of problem (15)–(17), we differentiate equation (17) with respect to time, and then, using equations (15) and (16), compose the following expression:

$$\left(1-\frac{s\dot{s}}{\nu}\right)\varphi(s,\tau)-s\left.\frac{\partial\varphi}{\partial\xi}\right|_{\xi=s}=g(\tau). \tag{18}$$

Here, the dot over the symbol denotes differentiation with respect to $\tau$. Taking advantage again of the shallowness of the molten pool and expanding the unknown function $\varphi$ into the $\xi$-power series restricts the analysis to the quadratic approximation

$$\varphi(\xi,\tau)=\varphi_0(\tau)+\varphi_1(\tau)\xi+\varphi_2(\tau)\xi^2.$$

The coefficients $\varphi_0$, $\varphi_1$ and $\varphi_2$ are determined from equations (16)–(18):

$$\varphi_0=g(\tau),\quad \varphi_1=-3\frac{g(\tau)}{s(\tau)}\frac{2+b(\tau)}{4+b(\tau)},$$

$$\varphi_2=2\frac{g(\tau)}{s^2(\tau)}\frac{b(\tau)}{4+b(\tau)}$$

where $b(\tau)=s\dot{s}/\nu$. This finally yields:

$$v_r=VW_1,\quad v_z=-UyW_2-SVW_3 \tag{19}$$

where

$$V=\frac{Sf}{6(4+b)}$$

$$U=\frac{1}{3(4+b)}\left[\frac{S^2f}{2r}+Sf\frac{\partial S}{\partial r}+\frac{1}{2}S^2\frac{\partial f}{\partial r}-\frac{S^2f}{2(4+b)}\frac{\partial b}{\partial r}\right]$$

$$W_1=-6-b+6(4+b)y-9(2+b)y^2+4by^3$$

$$W_2=-6-b+3(4+b)y-3(2+b)y^2+by^3$$

$$W_3=y\left[\frac{6+b}{S}\frac{\partial S}{\partial r}-\frac{\partial b}{\partial r}+3y\left(\frac{\partial b}{\partial r}-2\frac{4+b}{S}\frac{\partial S}{\partial r}\right)\right.$$
$$\left.-3y^2\left(\frac{\partial b}{\partial r}-3\frac{2+b}{S}\frac{\partial S}{\partial r}\right)+y^3\left(\frac{\partial b}{\partial r}-4\frac{b}{S}\frac{\partial S}{\partial r}\right)\right]$$

$$y=\frac{z}{S(r,t)}$$

$$b=\frac{s\dot{s}}{\nu}.$$

The flow of the melt has a vortex structure. In the region near the centre of the heating spot the liquid moves to the surface, whereas on the free surface, $z=0$, it moves from the centre to the pool edges (Fig. 1), since with $\alpha>0$ the thermocapillary force is directed to the side of decreasing temperature. Should the surface tension increase with temperature, then $\alpha<0$ and the signs of $v_r$ and $v_z$ in equation (19) reverse, and the liquid in this case will move in the opposite direction. By solving the equation $v_r=0$ in $y$ with the help of equation (19), the coordinate of the flow turning, $y_0=[18+5b-(9b^2+84b+324)^{1/2}]/8b$, can be found. The analysis of this formula shows that the value of $y_0$ depends weakly on $r$ and $t$ and is approximately equal to 0.33 (the dashed line in Fig. 1). The vortex is highly flattened in the direction of the $z$ axis, thus corresponding to the initial assumption that $v_z \ll v_r$; except for the narrow regions near the centre of the heating spot $r=0$ and near the points of the flow turning $y=y_0$ the liquid moves virtually parallel to the surface $z=0$.

The variation in time of the shape and dimensions of the molten pool bottom leads to the following

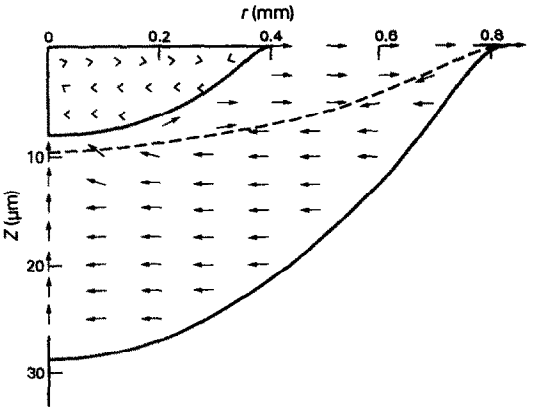


FIG. 1. The field of flow velocity vector directions in the melting of titanium ($q_0=5\times10$ W cm$^{-2}$, $k=100$ cm$^{-2}$), $t=0.47$ (>) and 1 μs (→).

interesting feature of the phenomenon considered. In a pool with an immovable bottom, the region in which the flow velocity differs notably from zero has the dimension $\Delta z \sim \sqrt{(\nu(t-t_m))}$ (this follows from the parabolic-type equation (15)), i.e. when $t \to t_m$ the liquid is quiescent in the entire melt except for a thin layer of thickness $\Delta z$ near the surface $z = 0$. In the considered problem with the moving bottom of the pool, the velocity of the melt has the same order of magnitude over the entire liquid phase except for a narrow layer near the melting front and at the vortex centre. This is due to the fact that at the start of melting the depth of the pool is zero, i.e. its bottom coincides with the free surface $S(r, t_m) = 0$, with the melting front velocity $\partial S/\partial t$ also being equal to zero at $t = t_m$ [17]. Therefore, the growth rate of the zone of influence of the thermocapillary force $d\Delta z/dt$ considerably exceeds the rate of increase in the molten pool dimensions when $t \to t_m$. Thus, the liquid over the entire pool responds instantly to the presence of the thermocapillary force which sets the liquid into motion.

Before going over to the analysis of the mass transfer of doping elements from the surface $z = 0$ into the melt volume, note that the admixture can reach the bottom of the pool only in the case when the maximum positive value $v_z^{max}$ (attainable at the point $r_m \simeq 3R(t)/4$, $z_m \simeq S(r_m, t)/3$) exceeds the velocity of the melting front $\partial S/\partial t$. It should be emphasized that this estimate affords only the necessary (but not sufficient) condition for deep mass transfer; a more detailed analysis requires the study of the trajectories of liquid particles.

Because of the unsteady-state character of the process of melting, the shape and dimensions of the vortex vary with time (Fig. 1). Consequently, the shape and dimensions of the trajectories of liquid particles change (Fig. 2). The characteristic features of the given process are the openness of the trajectories and the increase with time of the radius of their curvature due to the growth of the vortex. There are also particles of the melt the radius of the trajectory curvature of which decreases with time at a certain stage (inner curves in Figs. 2(a) and (c)). This takes place in a certain neighbourhood of the vortex centre which moves in the direction of increasing coordinates $r$ and $z$. The position of the vortex centre is described by the approximate relations $r_c \simeq R(t)/2$, $z_c \simeq S(r_c, t)/3$. So, some trajectories may turn to be intersecting (Fig. 2(c)). The particles of the melt that pass during their motion near the surface $z = 0$ perform convective mass transfer of the admixture which enters the melt from the surface following one mechanism or another. The final positions of the admixture particles may differ substantially after the termination of the laser pulse. For example, Fig. 2(a) depicts the paths of motion of elementary melt volumes initially located at a relatively small distance from one another. It is seen that there exist both points that return into the neighbourhood of the original location, and those

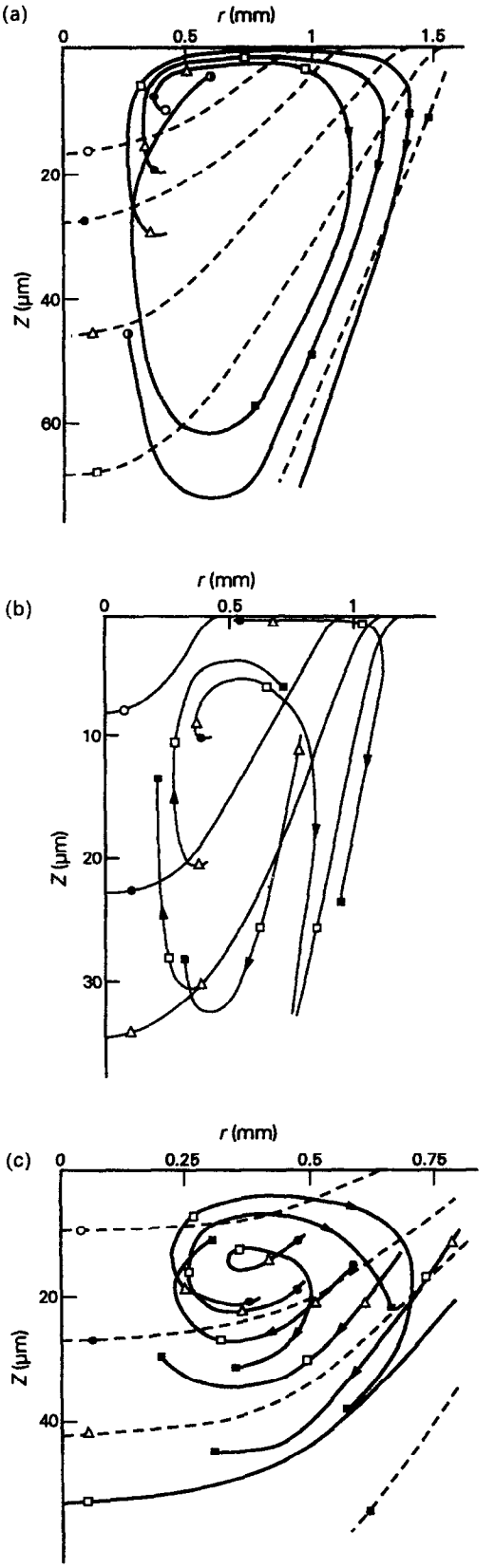


FIG. 2. The trajectories of the melt particles in melting of titanium. $t = 0.2$ μs (○); 0.4 (●); 0.6 (△); 1.0 (□); 1.6 (■); 2.3 (○). (a) $q_0 = 5 \times 10$ W cm$^{-2}$, $k = 50$ cm$^{-2}$; (b) $q_0 = 10^5$, $k = 100$; (c) $q_0 = 10^5$, $k = 150$.

which penetrate rather deeply into different regions of the molten pool, thus confirming the assumption about the possibility of a deep convective transportation of the admixture into the melt by thermocapillary fluxes. The admixture particles are transported into the material far from the heating spot centre where $v_z > 0$. Considerable spatial scattering of the final points of the trajectories (Figs. 2(a) and (b)) allows an assumption about the existence of lasing regimes that ensures both a relatively uniform and non-monotonous distribution of the admixture in the molten zone.

## THERMOCAPILLARY MASS TRANSFER OF THE ADMIXTURE

As a rule, the laser doping of metals is done from coatings, from a gas (liquid) phase or by introducing doping powder into the laser-affected zone. The mass transfer of admixture elements in this zone of lasing is simulated by the transfer of markers in the molten pool [19]. It will be assumed that the markers do not interact with the melt and with each other. It is seen from simple estimates that the characteristic distance over which the admixture is transported by the diffusion mechanism, $l_d \sim \sqrt{(Dt^*)} \sim 10^{-6}$ m ($D$ is the coefficient of diffusion of the doping element in the element being doped, $t^*$ is the time of lasing), is much smaller than that over which the admixture is transported by convection, $l_c \sim v_r t^* \sim 10^{-4}$ m ($v_r$ is the radial thermocapillary velocity of the melt in equations (19)). In view of this, the diffusive transport of markers in the molten pool is neglected in comparison with convective transfer. The technique by which the markers are introduced into the laser-affected zone corresponds to that used to introduce a doping component into a melt.

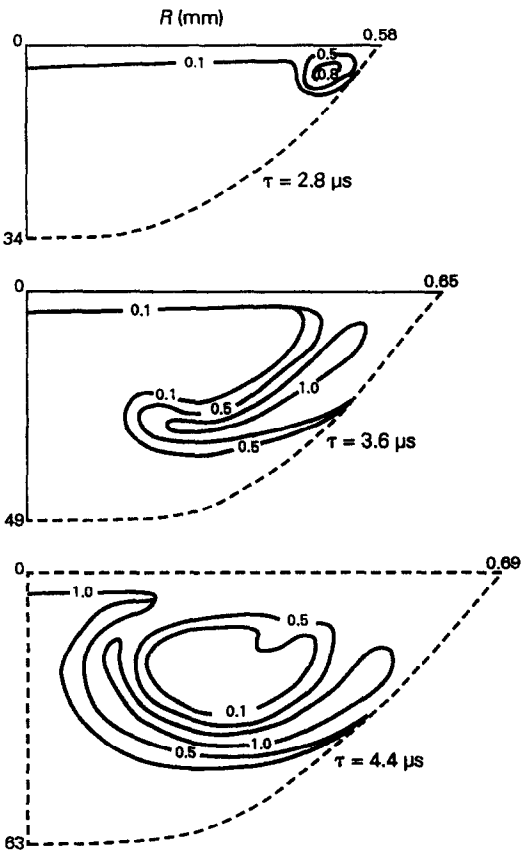


FIG. 3. The admixture concentration field for the time instants $t = 2.8$, 3.6 and 4.4 $\mu$s, respectively. Doping of titanium from the gas phase. The absorbed energy flux density $q_0 = 2.5 \times 10^4$ W cm$^{-2}$ and the concentration coefficient $k = 150$ cm$^{-2}$. The dashed line is the phase interface.

*Doping from the gas phase*

When metal is doped from the gas phase, a constant flux of the doping component exists on the free surface of the molten pool, i.e. not only does the redistribution of the admixture over the molten pool take place, but also an increase in the quantity of the doping substance in the laser-affected zone. Figure 3 demonstrates the concentration fields of the doping component in the case of pulse irradiation of titanium. To obtain a clearer picture, the values of concentration are normalized to the density of the doping gas.

At the initial stages of mass transfer the admixture is concentrated near the melt surface, with the region of the local maximum of concentrations (with a depth of about 10 $\mu$m and diameter equal to 0.1 of the heating spot diameter) being located in the periphery region near the edge of the pool. At this stage the admixture does not penetrate into the pool (Fig. 3, $t = 2.8$ $\mu$s). Such a structure of the admixture concentration field is characterized by the distribution of the doping component being practically in the plane of the free surface, with the region of maximum concentrations in the form of a ring near the edge of the melting zone.

As the time increases and the growth of the coordinate of the pool along the radius slows down, the admixture displaces from the region $S(r, z = 0, t)$ into the interior of the melt along the melting front, resulting in the transfer of the region of the maximum concentrations of the doping component from the surface zone inside the material and to the stretching of this zone along the liquid–solid interface (Fig. 3, $t = 3.6$ $\mu$s). Since at the initial stage of mass transfer the velocity of the melting front exceeds the axial velocity components of the melt, the region of propagation of the admixture separates from the phase interface and enters the zones with smaller axial velocity components. This leads to the exfoliation of the doped region from the melting front and results in the formation of the doping zone in the form of a strip propagating into the melt and to the centre of the molten pool, thus ensuring a deep penetration of the admixture.

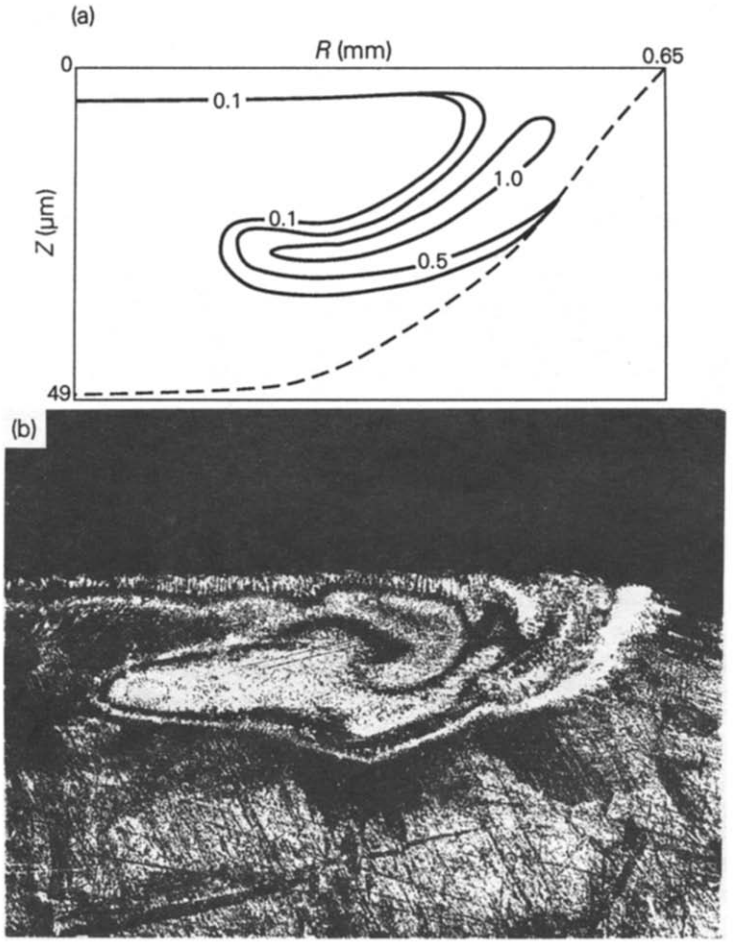


FIG. 4. (a) The admixture concentration field for the time instant $t = 3$ μs for doping of titanium from the gas phase. $q_0 = 5 \times 10^4$ W cm$^{-2}$, $k = 100$ cm$^{-2}$. (b) The microsection of the laser-affected zone in irradiation of iodide titanium in vapours of liquid nitrogen. $q_0 = 5 \times 10^4$ W cm$^{-2}$, $k = 100$ cm$^{-2}$ and the pulse duration is 5 μs.

Due to the vortical structure of the flow of the melt, the admixture displaces then to its free surface. By this time, the maximum depth of penetration of the doping component comprises about two-thirds of the pool depth. The circular structure of the doping zone with weak penetration of the admixture into the centre owes its origin solely to the eddying motion of the melt. For the considered laser radiation parameters within the ranges of the absorbed energy, flux density $q = 10^4$–$5 \times 10^4$ W cm$^{-2}$ and the coefficient of concentration $k = 50$–$200$ cm$^{-2}$, the formation of circular doped structures takes from 3 to 5 μs. The increase in the number of rotations performed by the admixture in the pool leads to an increase in the uniformity of the doping component distribution. However, the form of the concentration fields is described only qualitatively in this case.

In the works dealing with the laser synthesis of refractory metal nitrides [20, 21], different structures originating in the laser-affected zone are described. Their formation can be attributed to the presence of the circular doped region, with the following layers being located in succession over the pool depth: the surface layer enriched with the doping component (this layer corresponds to the zone where the admixture gains access); a layer near the centre of the vortex with weak penetration of the doping component; then a layer enriched with the doping due to the convective mass transfer from the surface and, finally, a layer depleted of the admixture owing to the separation of the region of the doped material from the melting front. Thus, Fig. 4 presents the predicted field of concentrations (Fig. 4(a)) and the experimental data (Fig. 4(b)) on the structure of the distribution of the admixture in the laser-affected zone.

Note that the local increase in the admixture concentration with increase in the depth of the pool (for example, the depth of 20 μm) in Fig. 4(a) is associated with the redistribution of the doping component from the surface into the interior of the melt according to the mechanism: to the periphery and inside the laser-affected zone.

*Doping from the previously deposited coating*

Consider the action of the laser pulse on the system 'substrata-coating'. If the coating layer thickness is small as compared with the depth of the molten pool, the averaged thermophysical properties and the viscosity of the melt differ little from the corresponding parameters of the substrate metal. Otherwise one should consider thermocapillary convection in a two-layered system. The surface properties of the melt can differ substantially, even in the case of small concentrations of the admixture applied to the surface. However, if the redistribution of the coating from the surface of the irradiated material takes place for times smaller than the characteristic time of lasing, while the values of $d\sigma/dT$ for the coating and substrata differ little and have the same sign, the effect of the admixture concentration on the thermocapillary phenomena is not important. Then, the presence of the doping component on the free surface of the melt may introduce quantitative rather than qualitative differences into the dynamics of convective mass transfer. Thus, the difference between the thermophysical and surface properties of the material of the coating and substrate is neglected.

Figure 5 presents a comparison between the structures of concentrational fields of the admixture in the lasing zone for the computational (Fig. 5(a)) and full-scale (Fig. 5(b)) experiments. The surfaces of specimens fabricated from 3 mm thick armco–iron were coated with 30 $\mu$m thick molybdenum. The two-layer systems were treated with the help of an Nd-laser which generated 4 $\mu$s monopulses in the free generation mode with energy of 5–15 J and wavelength of 1.06 $\mu$m. When being irradiated, the specimens were blown with argon.

The X-ray spectral analysis of the distribution of the doping element across the laser-affected zone was made on the Kameka set-up 'Microbim' at an accelerating voltage of 15 kV and probe current of 20 nA. The thin structure was studied after preliminary thin etching from half-tone images recorded with the help of a four-pole detector of electrons which made it possible to reveal the chemical inhomogeneity of the molten pool. The chemical inhomogeneity was studied with the aid of an energy-dispersive LINK 860-500 spectrometer.

To different time instants in Fig. 5(a) there correspond different irradiation energies in Fig. 5(b). The increase in the irradiation energy leads to the increase in the temperature gradient on the melt surface and, consequently, to the enhanced thermocapillary motion of the liquid phase; on the other hand, the value of the melt velocity is a rapidly increasing function of time. Thus, both these factors—the increase of the laser radiation energy and the increase of time of lasing—lead to enhanced agitation of the melt, and this is manifested in analogous trends of mass transfer of the doping element. The radiation energy was varied in the full-scale experiment and the time of lasing in the computational experiment.

At the initial stages of mass transfer the admixture is concentrated in the coating. Due to the eddy character of melt motion, the doping component is transferred from the centre to the edges of the laser-affected zone. This leads to the formation of a zone of increased concentration displaced to the pool edge. As the radius of the melted pool increases, the admixture penetrates deep into the liquid phase along the melting front (Fig. 5(a), $t = 1.6$ $\mu$s). Such a redistribution of the simulated doping component leads to the surface of the irradiated material being freed from the previously applied coating in all the surface regions of the laser-affected zone except for the periphery. The results of the X-ray spectral microanalysis of this zone of lasing with a similar structure of the doped region are presented in Fig. 5(b) for the irradiation energy $E = 7$ J and are listed in Table 1. The concentration of molybdenum in the surface layers of the remelted zone (points 1 and 2) is lower than in the zone of doping in the depth of the pool (point 3). This quali-

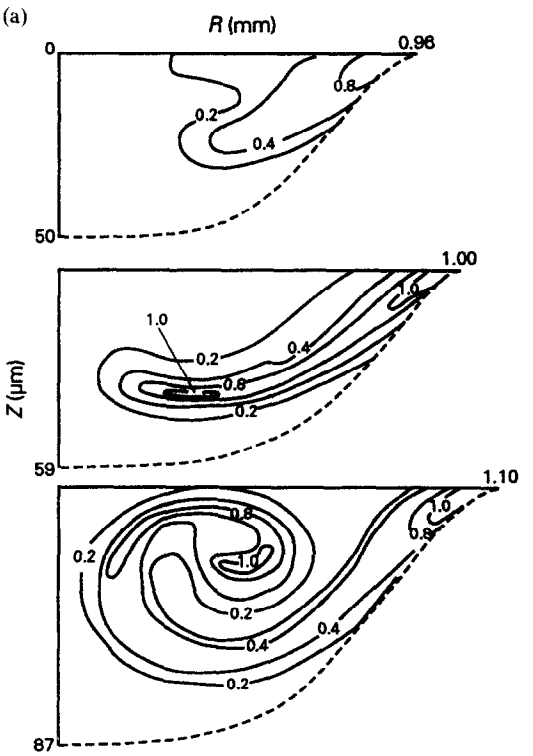


FIG. 5. Doping from the previously applied coating. (a) The admixture concentration field for the time instants $t = 1.6$, 1.9 and 2.8 $\mu$s. $q_0 = 5 \times 10^4$ W cm$^{-2}$, $k = 100$ cm$^{-2}$ and coating thickness $h = 15$ $\mu$m. (b) Microsections of the laser-affected zone in the two-layer coating of armco–iron-molybdenum. The thickness of the coating (molybdenum) $h = 30$ $\mu$m, the time of lasing $t = 4$ $\mu$s, the focusing spot radius $r = 1.5$ mm, and radiation energy $E = 7$, 7 and 10 J, respectively.

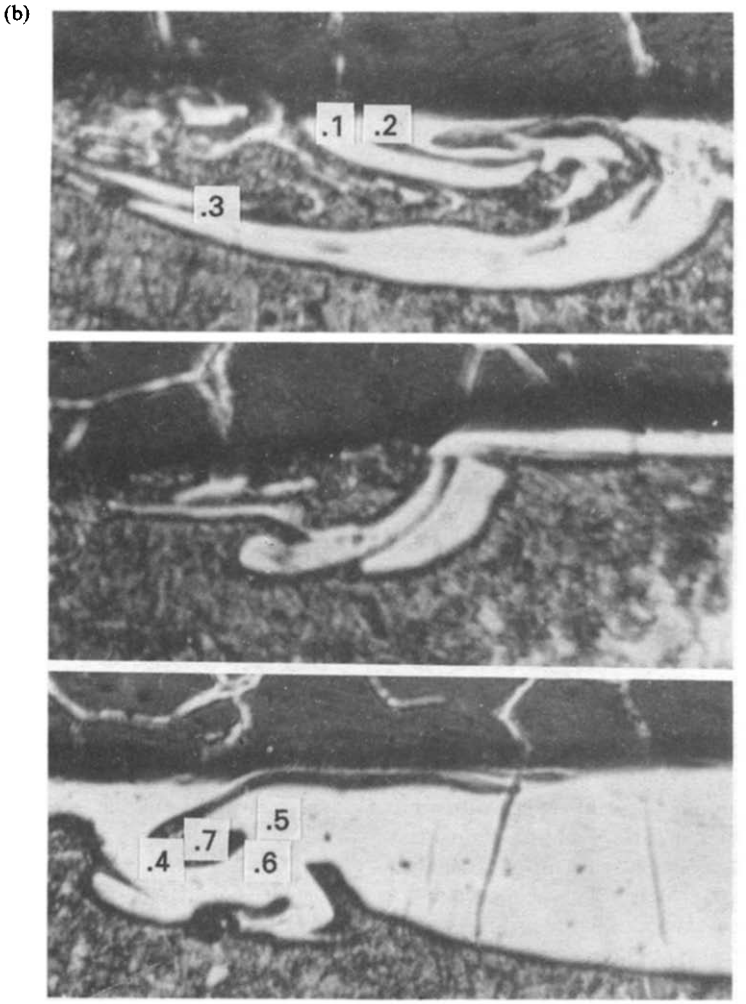


FIG. 5(b).

Table 1. X-ray spectral microanalysis of the laser-affected zone; doping of armco-iron with molybdenum from a 30 $\mu$m thick coating

| No. of point | 1 | 2 | 3 | 4 | 5 | 6 | 7 |
|---|---|---|---|---|---|---|---|
| Content of molybdenum, wt % | 28 | 12 | 44 | 64 | 28 | 32 | 6 |

tatively agrees with the predicted results. In this case the region near the surface of the remelted zone is partially freed from the previously applied coating. The excess of concentration of molybdenum at point 3 can be attributed to the redistribution of the admixture from the pool by the mechanism of thermocapillary convection.

In Fig. 5(a) it is shown for the time instant $t = 1.9$ $\mu$s that near the edge of the pool the region of doping is formed in the form of a strip which propagates into the interior and to the centre of the molten pool along the streamlines of the liquid phase. The admixture transferred from the surface is concentrated at the edge of the doping region. This leads to a local increase in its concentration in the laser-affected zone. Figure 5(b) presents the photograph of the microsection of the irradiated zone, the structure of which corresponds to the structure shown in Fig. 5(a) at $t = 1.9$ $\mu$s. The region near the heating spot centre is fully free from the coating layer.

Since at the initial stages of melting the phase interface velocity exceeds the value of the axial projection of the velocity of the melt, there occurs the separation of the simulated region of doping from the pool bottom. The propagation of the doped zone in the molten pool is monotonous until the markers arrive at the vortex centre. Here, the liquid phase velocity vector changes its direction and, consequently, the doping zone acquires the form of a coiling spiral (Fig. 5(a), $t = 2.8$ $\mu$s). The results of the experiment for regions of this type of doping are presented in Fig. 5(b) for the irradiation energy $E = 10$ J. The anomalous excess of the concentration of molybdenum

(point 4) over the mean concentration (points 5 and 6) in the remelting region corresponds qualitatively to the increase in the concentration at the apex of the spiral-like structure of the doped zone (Fig. 5(a), $t = 2.8$ $\mu$s). The position of the minimum concentration in the photograph (point 7) coincides with the predicted minimum of concentration in the zone free from the admixture near the vortex centre. This region of the minimum has an arc exit to the surface of the laser-affected zone just as in Fig. 5(a) at $t = 2.8$ $\mu$s.

It should be noted that in the case when the density of the absorbed energy flux is distributed by the Gaussian law, the size of the thermocapillary cell coincides with that of the pool. In the real experiment, the region of the pool edge is the region where the temperature gradient is always present during the entire time of irradiation. Therefore, despite the possible fluctuations of the incident energy flux in time and space, in the peripheral region of the laser-affected zone one can observe doped zones within the structure in the form of strips or spirals depending on the lasing parameters resulting from the thermocapillary agitation of the melt. Thus, in the range of irradiation parameters considered, with evaporation being insignificant, the thermocapillary mechanism of mass transfer in the regions of the remelting zone is a basic one which determines the structure of the doping zone.

The excess of the doping element concentration in the regions far from the surface of the irradiated material over those in the neighbourhood can be associated with convective transfer of the coating elements from the central regions to the periphery and with the pulling of them into the interior and to the centre of the molten pool at the initial stages of melting.

## REFERENCES


1. N. N. Rykalin, A. A. Uglov, I. V. Zuev and I. V. Kokora, *Laser and Electron Beam Material Processing*. Mir, Moscow (1988).
2. T. R. Anthony and H. E. Cline, Surface rippling induced by surface-tension gradients during laser surface melting and alloying, *J. Appl. Phys.* **48,** 3888–3894 (1977).
3. H. A. Papazian, Calculation of surface tension temperature coefficients, *Scripta Metall.* **18,** 1401–1403 (1984).
4. M. E. Glicksman, Interaction of flows with the crystal–melt interface, *Ann. Rev. Fluid Mech.* **18,** 307–335 (1986).
5. C. R. Heiple and J. R. Roper, Effect of selenium on GTAW fusion zone geometry, *Weld. J.* **60**(8), 143s–145s (1981).
6. C. R. Heiple and J. R. Roper, Mechanism for minor element effect on GTA fusion zone geometry, *Weld. J.* **61**(4), 97s–102s (1982).
7. A. G. Kirdyashkin, Thermogravitational and thermocapillary flows in a horizontal liquid layer under the conditions of a horizontal temperature gradient, *Int. J. Heat Mass Transfer* **27,** 1205–1218 (1984).
8. J. C. Loulergue, Deformation of surfaces of a thin liquid film by thermal perturbation, *Thin Solid Films* **82,** 61–71 (1981).
9. C. S. Yih, Fluid motion induced by surface-tension variation, *Physics Fluids* **11,** 477–480 (1968).
10. C. L. Lai and A. T. Chai, Surface temperature distribution along a thin liquid layer due to thermocapillary convection, *Acta Astronautica* **13**(11/12), 655–659 (1986).
11. R. V. Birikh, Concerning the thermocapillary convection in a horizontal fluid layer, *Zh. Prikl. Mekh. Tekh. Fiz.* No. 3, 69–72 (1966).
12. A. G. Kirdyashkin, Thermocapillary periodic flows, *Int. J. Heat Mass Transfer* **30,** 109–124 (1987).
13. A. Zebib, G. M. Homsy and E. Meiburg, High Marangoni number convection in a square cavity, *Physics Fluids* **28,** 3467–3476 (1985).
14. J. Srinivasan and B. Basu, A numerical study of thermocapillary flow in rectangular cavity during laser melting, *Int. J. Heat Mass Transfer* **29,** 563–572 (1986).
15. M. Strani, R. Piva and G. Graziani, Thermocapillary convection in a rectangular cavity: asymptotic theory and numerical simulation, *J. Fluid Mech.* **130,** 347–376 (1983).
16. A. K. Sen, Thermocapillary convection in a rectangular cavity with a deformable interface, *Physics Fluids* **29,** 3881–3884 (1985).
17. A. A. Uglov, I. Yu. Smurov and A. G. Gus'kov, Calculation of melting of metals by the concentrated energy flux, *Fiz. Khim. Obrab. Materialov* **19**(3), 3 8 (1985).
18. A. A. Uglov, I. Yu. Smurov and A. M. Lashin, Simulation of the unsteady-state motion of phase boundaries on the action of energy fluxes on materials, *Teplofiz. Vysok. Temp.* **27**(1), 87–93 (1989).
19. R. W. Hockney and J. W. Eastwood, *Computer Simulation Using Particles*. McGraw-Hill, New York (1981).
20. A. A. Uglov, M. B. Ignatiyev and I. Yu. Smurov, Laser-plasma synthesis of Ti and Zr nitrides, *Fiz. Khim. Obrab. Materialov* No. 2, 88–91 (1987).
21. M. B. Ignatiyev, V. I. Titov, I. V. Melekhin, V. V. Hangulov, S. B. Maslenkov and A. P. Stepanov, The laws governing the mass transfer of the doping component in the processes of laser micrometallurgy. In *Physicochemical Processes of the Processing of Materials by Concentrated Energy Fluxes*, pp. 37–46. Izd. Nauka, Moscow (1989).


## SIMULATION DU TRANSFERT DE MASSE THERMOCAPILLAIRE VARIABLE PAR DOPAGE LASER DES METAUX


**Résumé**—Sous les approximations d'un bain fondu peu profond, d'un nombre de Reynolds réduit faible et d'une surface libre plane, on considère l'écoulement de fusion thermocapillaire variable pour le cas de la fusion d'un corps solide par une source de chaleur gaussienne. Basé sur le champ de vitesse obtenu, le transfert convectif de masse de l'impureté dopante est analysée par la méthode des particules dans l'hypothèse d'un petit nombre de Schmidt. On montre la faisabilité d'une production de structures, à la fois relativement homogènes et principalement non monotones, de champs de concentration dans la zone refondue. On fait l'analyse de la formation de telles structures et on révèle leur particularité dans le cas du dopage laser des métaux depuis la phase gazeuse (plasma) et les revêtements préalablement déposés. On compare les profils de concentration prédits et les résultats expérimentaux et on obtient un accord qualitatif satisfaisant.

## SIMULATION DES INSTATIONÄREN THERMOKAPILLAREN STOFFTRANSPORTS BEI DER BEARBEITUNG METALLISCHER OBERFLÄCHEN MITTELS LASER

**Zusammenfassung**—Unter der Annahme eines flachen Schmelzbades, kleiner reduzierter Reynolds-Zahlen und einer ebenen, freien Oberfläche wird die instationäre thermokapillare Strömung einer Schmelze untersucht. Dies geschieht für das Schmelzen eines metallischen Körpers mit Hilfe einer Gauß'schen Oberflächen-Wärmequelle. Aufgrund des ermittelten Geschwindigkeitsfeldes wird der konvektive Stofftransport der eingebrachten Verunreinigung mit dem Verfahren von Modellpartikeln unter Annahme einer kleinen Schmidt-Zahl untersucht. Es wird die Möglichkeit aufgezeigt, entweder eine relativ homogene oder aber eine im wesentlichen nicht monotone (geschichtete) Struktur des Konzentrationsfeldes im aufgeschmolzenen Gebiet herzustellen. Die Bildung solcher Strukturen wird analysiert, und ihre besonderen Merkmale werden für den Fall gezeigt, daß die Metalloberfläche mittels Laser behandelt wird—entweder aus der Gas- (Plasma-) Phase oder aus zuvor aufgebrachten Beschichtungen. Die berechneten Konzentrationsprofile werden mit Versuchsergebnissen verglichen, wobei sich eine zufriedenstellende qualitative Übereinstimmung ergibt.

## МОДЕЛИРОВАНИЕ НЕСТАЦИОНАРНОГО ТЕРМОКАПИЛЛЯРНОГО МАССОПЕРЕНОСА ПРИ ЛАЗЕРНОМ ЛЕГИРОВАНИИ МАТЕРИАЛОВ

**Аннотация**—В приближении мелкой ванны расплава, малого приведенного числа Рейнольдса и плоской свободной поверхности рассмотрено нестационарное термокапиллярное течение расплава при плавлении массивного металлического тела гауссовым поверхностным тепловым источником. На основании полученного поля скоростей методом модельных частиц проанализирован конвективный массоперенос легирующей примеси в предположении малости числа Шмидта. Показана возможность немонотонных (слоистых) структур концентрационных полей в переплавленной зоне. Выполнен анализ образования и выявлены качественные особенности таких структур при лазерном легировании металлов из газовой (плазменной) фазы и из предварительно нанесенных покрытий. Проведено сравнение полученных концентрационных профилей с результатами экспериментов и обнаружено их удовлетворительное качественное совпадение.